156. Novel nanoparticles composition

(University of Pennsylvania)

5TH KDDF GLOBAL C&D TECH FAIR

Asset Overview

Product Type	Antibody + Nanoparticle
Disease Area	Inflammatory Disease
Indication	Acute Inflammatory Disease
Current Stage	Lead Optimization
Target	Neutrophils in Acute Lung Inflammation (ALI)
MoA	Arrangement of protein in or on the nanoparticles via hydrophobic interactions, crosslinking and electrostatic interactions
Brief Description	• Acute inflammatory diseases, including sepsis, pneumonia, and acute respiratory distress syndrome (ARDS), account for over 1.5 million hospitalizations and 300,000 deaths per year in the US. These diseases all share a common cellular player known as marginated leukocytes. • Marginated leukocytes are white blood cells that accumulate in the blood vessels of inflamed organs and potentiate disease progression by releasing toxins and pro-inflammatory cytokines and induce clotting and further inflammation. Accumulation of marginated leukocytes can ultimately lead to organ dysfunction. • Inventors developed a molecular label consisting of an IgG antibody bound to dibenzocyclooctyne (D20 tag). When attached to nanoparticles, the D20 tag almost exclusively localized to marginated leukocytes to alleviate disease symptoms in a small animal model of acute inflammatory injury. • Using the D20 tag to target marginated leukocytes with imaging agents or drugs could better enable clinical diagnosis and treatment of acute inflammatory diseases.
Intellectual Property	WO2021/113519A1
Publication	Supramolecular Arrangement of Protein in Nanoparticle Structures Predicts Nanoparticle Tropism for Neutrophils in Acute Lung Inflammation. Nat Nanotechnol. (2022)
Inventors	Priyal PATEL, Jacob Myerson, Jacob BRENNER, Vladimir R. Muzykantov, Landis R. WALSH

Highlights

- Provides ~ 50% more protection against cellular leakage than non-tagged nanoparticles following inflammatory injury, which is key for alleviating acute inflammatory disease progression
- Provides ~ 2x specificity to inflamed lung tissue versus heart, liver, spleen, and kidneys following inflammatory lung injury, which is key for accurately diagnosing and effectively treating acute inflammatory diseases
- Compatible with liposomes for small molecule drug or imaging agent delivery and solid lipid nanoparticles for modified mRNA delivery

156. Novel nanoparticles composition

(University of Pennsylvania)

Key Data

Lysozyme–dextran NGs and crosslinked albumin NPs accumulate in marginated neutrophils in inflamed lungs

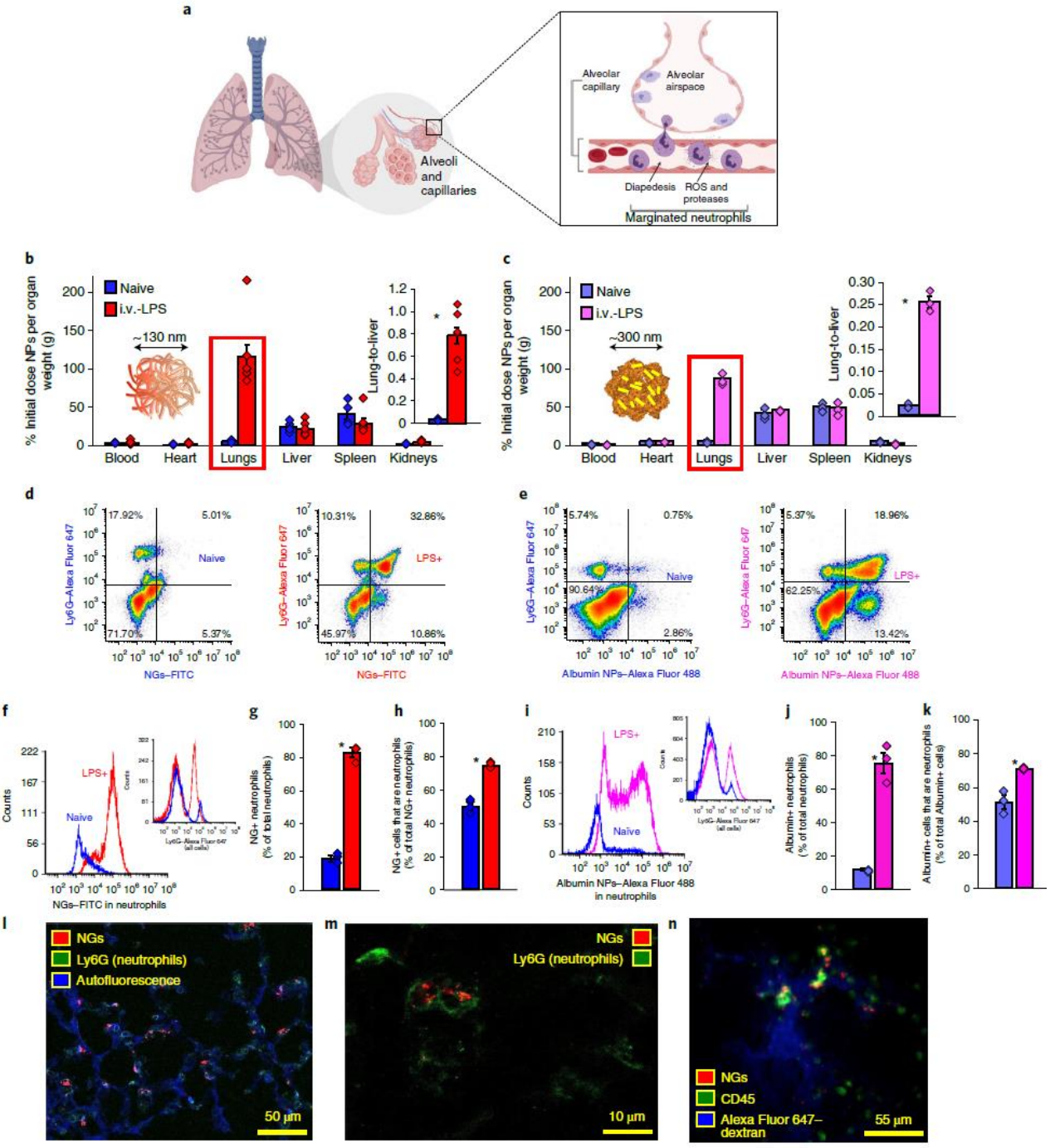

To be continued

Key Data

Lysozyme–dextran NGs and crosslinked albumin NPs accumulate in marginated neutrophils in inflamed lungs

a, Schematic of neutrophil margination and extravasation in inflamed lungs (created with BioRender.com). ROS, reactive oxygen species. **b**, Biodistributions of lysozyme–dextran NGs in naive (n = 4 animals) and i.v.-LPS-affected (n = 8 animals) male C57BL/6 mice (red box, $P < 1 \times 10{-}10$; $^*P = 0.00008$). Inset: ratio of nanoparticle uptake in the lungs to nanoparticle uptake in the liver. **c**, Biodistributions of PEG–*N*-hydroxysuccinimide crosslinked human albumin NPs in naive (n = 3 animals) and i.v.-LPS-injured (n = 3 animals) mice (red box, $P < 1 \times 10{-}10$; $^*P = 0.004$). Inset: ratio of nanoparticle uptake in the lungs to nanoparticle uptake in the liver. **d–k**, Flow cytometry characterization of single-cell suspensions prepared from naive and i.v.-LPS-affected mouse lungs. Vertical axis in **d** and **e** indicates Ly6G staining for neutrophils and horizontal axis indicates signal from fluorescent NGs (**d**) or fluorescent albumin NPs (**e**). NG (**f**) and albumin NP (**i**) fluorescent signal from neutrophils in i.v.-LPS-injured mouse lungs (red/pink), compared to naive lungs (blue). Insets in **f** and **i**: flow cytometry data verifying increased neutrophil concentration in i.v.-LPS-injured mouse lungs (red/pink). Fraction of neutrophils positive for NGs (**g**) or albumin NPs (**j**) in naive or i.v.-LPS-injured lungs and fraction of NG-positive (**h**) or albumin NP-positive (**k**) cells that are neutrophils. For **g** and **h**, NGs/naive: n = 4 animals, NGs/LPS: n = 4 animals. For **j** and **k**, albumin NPs/naive: n = 3 animals, albumin NPs/LPS: n = 3 animals. $^*P = 2.6 \times 10{-}7$ (**g**), $^*P = 1.7 \times 10{-}5$ (**h**), $^*P = 0.0006$ (**j**), $^*P = 0.007$ (**k**). For **l** and **m**, fluorescence micrographs indicating association of NGs (red) with neutrophils (green, Ly6G stain) in the lungs of an i.v.-LPS-affected mouse (blue, tissue autofluorescence). Data are from histology for two naive mice and two i.v.-LPS-affected mice. **l**, Broad field of view indicating neutrophils and NGs alongside lung anatomy. **m**, Narrow field of view showing two neutrophils containing NGs. **n**, Single frame from real-time intravital imaging of NG (red) uptake in leukocytes (green) in the lungs of one i.v.-LPS-affected mouse (blue, Alexa Fluor 647-dextran). Statistical significance in **b** and **c** is derived from two-way analysis of variance (ANOVA) with Sidak's multiple-comparisons test. Statistical significance in **g**,**h**,**j**,**k** is derived from paired two-tailed t tests. All error bars indicate mean ± s.e.m.

156. Novel nanoparticles composition

(University of Pennsylvania)

Key Data

Screen of diverse NP biodistributions in naive and i.v.-LPS-affected lungs

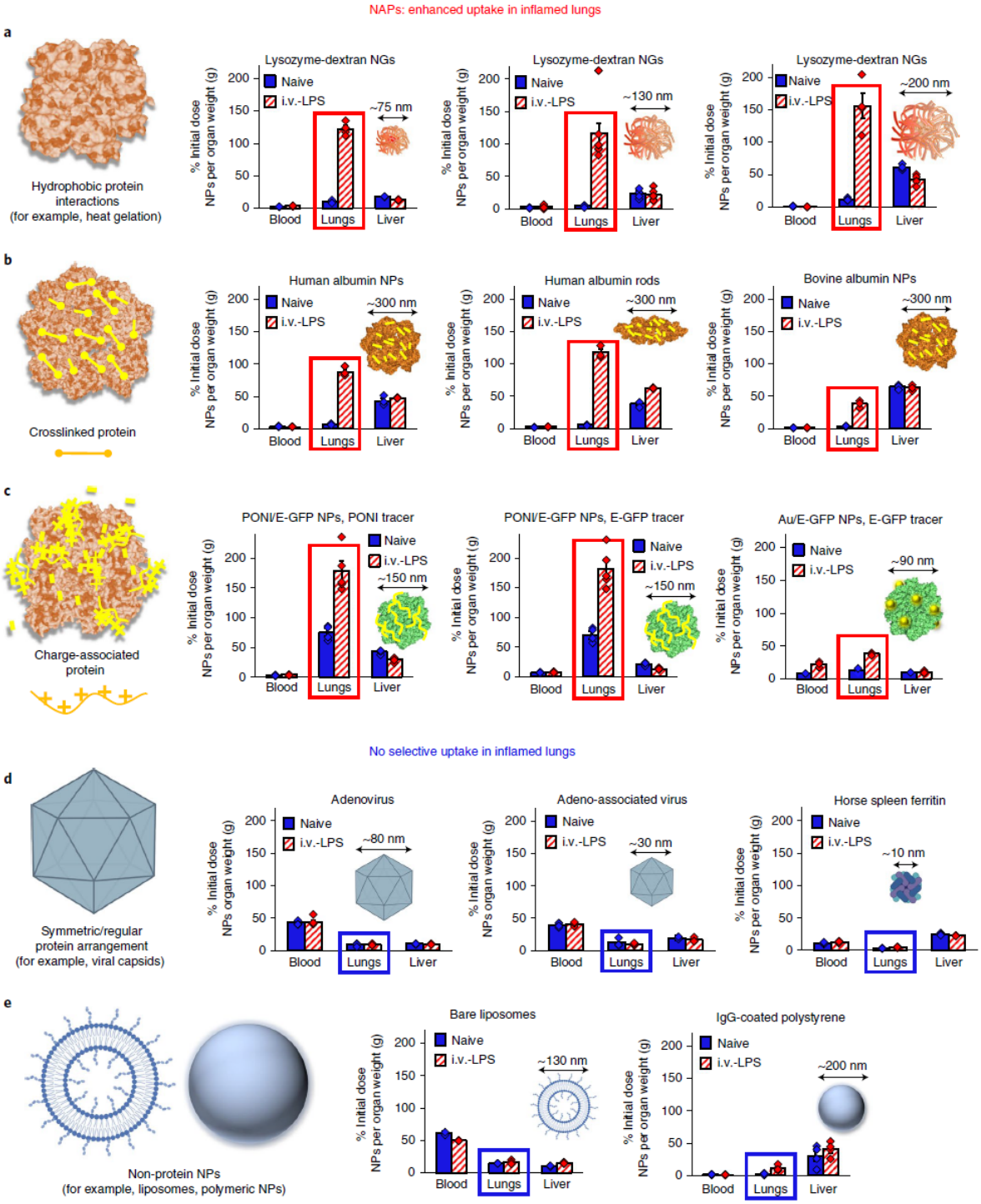

To be continued

Key Data

Screen of diverse NP biodistributions in naive and i.v.-LPS-affected lungs

a–c, NAPs accumulate in acutely inflamed lungs. **a**, Biodistributions of variant NGs indicating uptake of 75 nm NGs (n = 4 i.v.-LPS animals, n = 4 naive animals, red box: $P < 1 \times 10{-}10$) and 200 nm NGs (n = 5 i.v.-LPS, n = 5 naive, red box: $p < 1 \times 10{-}10$) in LPS-injured lungs, but not naive lungs. Data for 130 nm NGs are identical to that presented in Fig. 1b. **b**, Biodistributions of variant crosslinked albumin NPs indicating uptake of albumin nanorods (n = 3 i.v.-LPS animals, n = 3 naive animals; red box, $P < 1 \times 10{-}10$) and bovine albumin NPs (n = 3 i.v.-LPS animals, n = 3 naive animals; red box, $P < 1 \times 10{-}10$) in LPS-injured, but not naive lungs. Data for human albumin nanoparticles are identical to that presented in Fig. 1c. **c**, Biodistributions of charge-agglutinated protein NPs, indicating uptake of particles comprised of E-GFP and guanidine-tagged PONI or particles comprised of E-GFP and guanidine-tagged gold nanoparticles in LPS-injured (PONI: n = 5 animals; Au: n = 3 animals), but not naïve (PONI: n = 4 animals; Au: n = 3 animals) lungs. PONI/E-GFP data reflect tracing of both 131I-labelled PONI and 125I-labelled E-GFP. For PONI tracer data: red box, $P < 1 \times 10{-}10$. For E-GFP tracer data: red box, P = 0.0003. For Au/E−GFP data: red box, $P = 1.6 \times 10{-}9$. **d**, NPs based on symmetric supramolecular arrangement of protein do not have tropism for inflamed lungs (schematics created with BioRender.com). Biodistributions of adenovirus (n = 5 i.v.-LPS animals, n = 5 naive animals; blue box, P = 0.88), adeno-associated virus (n = 3 i.v.-LPS animals, n = 3 naive animals; blue box, P = 0.56) and ferritin nanocages (n = 5 i.v.-LPS animals, n = 5 naive animals; blue box, P = 0.35) indicating no selectivity for LPS-injured versus naive lungs. **e**, Biodistributions of bare liposomes (schematic created with BioRender.com, n = 4 i.v.-LPS animals, n = 4 naive animals) indicating no selectivity for LPS-injured versus naïve lungs (blue box, P = 0.31). Biodistributions of IgG-coated polystyrene NPs indicating low levels of uptake in both naive (n = 4 animals) and LPS-injured (n = 4 animals) lungs (blue box, P = 0.0004). Statistical significance in all panels is derived from two-way ANOVA with Sidak's multiple comparisons test. All error bars indicate mean ± s.e.m.

156. Novel nanoparticles composition

(University of Pennsylvania)

Key Data

Engineering of liposome surface chemistry to confer NAP-like behaviour in LPS-inflamed lungs

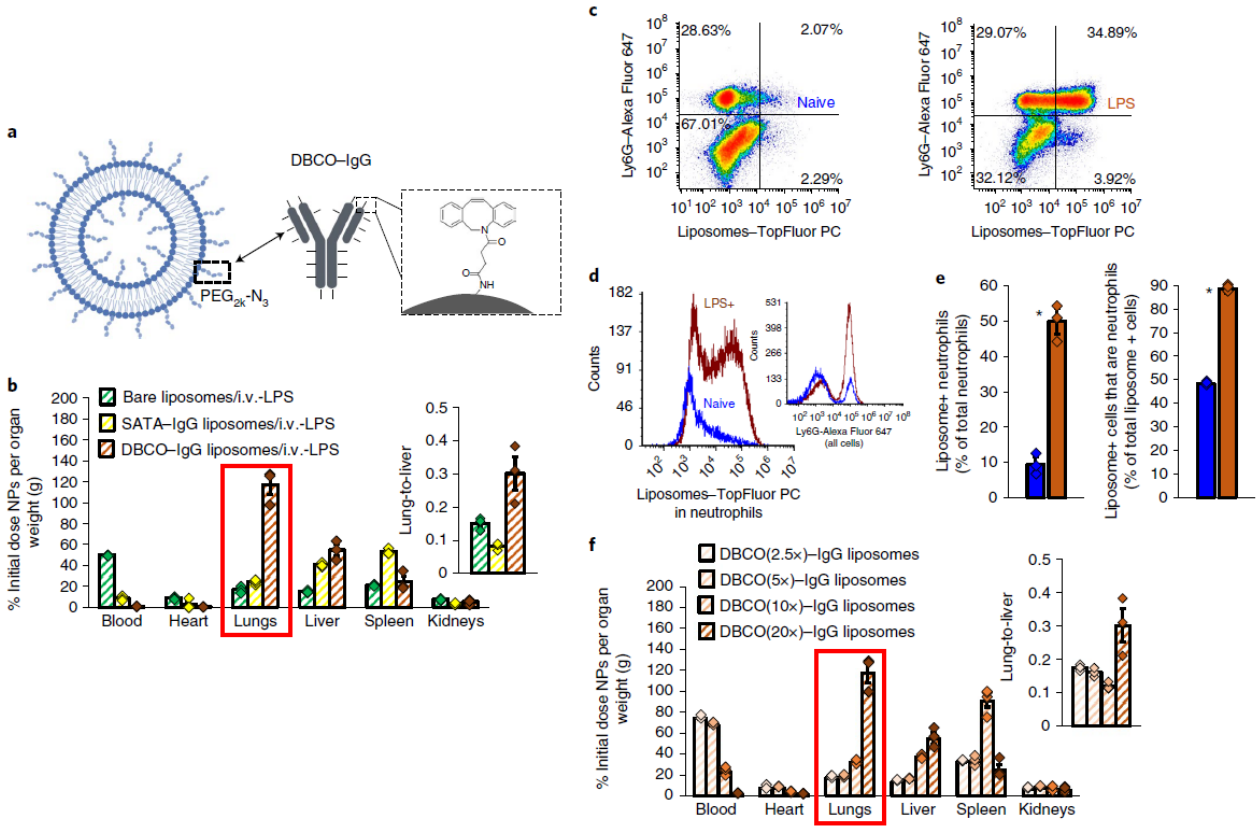

a, Schematic of antibody-coated liposomes prepared via copper-free click reaction of azide-functionalized liposomes with DBCO-functionalized IgG (liposome schematic created with BioRender. com). **b**, Biodistributions in i.v.-LPS-injured mice for bare liposomes (n = 3 animals), liposomes conjugated to IgG via SATA-maleimide chemistry (n = 3 animals) and liposomes conjugated to IgG via DBCO–azide chemistry (n = 3 animals) (red box, $P < 1 \times 10-10$ for DBCO–IgG liposomes versus bare liposomes and DBCO–IgG liposomes versus SATA–IgG liposomes). **c**, Mouse lung flow cytometry data indicating Ly6G anti-neutrophil staining density versus levels of DBCO–IgG liposome uptake as indicated by the green fluorescent TopFluor PC lipid signal. **d**, Flow cytometry data verifying increased DBCO–IgG liposome uptake in and selectivity for neutrophils following LPS insult. Inset: verification of increased concentration of neutrophils in the lungs following LPS. **e**, Fraction of neutrophils positive for DBCO–IgG liposomes in naive (n = 3 animals) or i.v.-LPS-injured (n = 3 animals) lungs ($*P$ = 0.0003) and fraction of DBCO–IgG liposome-positive cells that are neutrophils ($*P = 1.7 \times 10-6$). **f**, Biodistributions in i.v.-LPS-injured mice for azide-functionalized liposomes conjugated to IgG loaded with 2.5 (n = 3 animals), 5 (n = 3 animals), 10 (n = 4 animals) and 20 DBCO molecules per IgG (n = 3 animals; red box, $P < 1 \times 10-10$ for DBCO(20×)–IgG liposomes compared to each of the other DBCO density groups). Insets in **b** and f: ratio of NP uptake in the lungs to NP uptake in the liver. Statistical significance in **b** and **f** is derived from two-way ANOVA with Tukey's multiple-comparisons test. Statistical significance in **e** is derived from paired two-tailed t tests. All error bars indicate mean ± s.e.m.

156. Novel nanoparticles composition

(University of Pennsylvania)

Key Data

Effects of NAPs in model ARDS

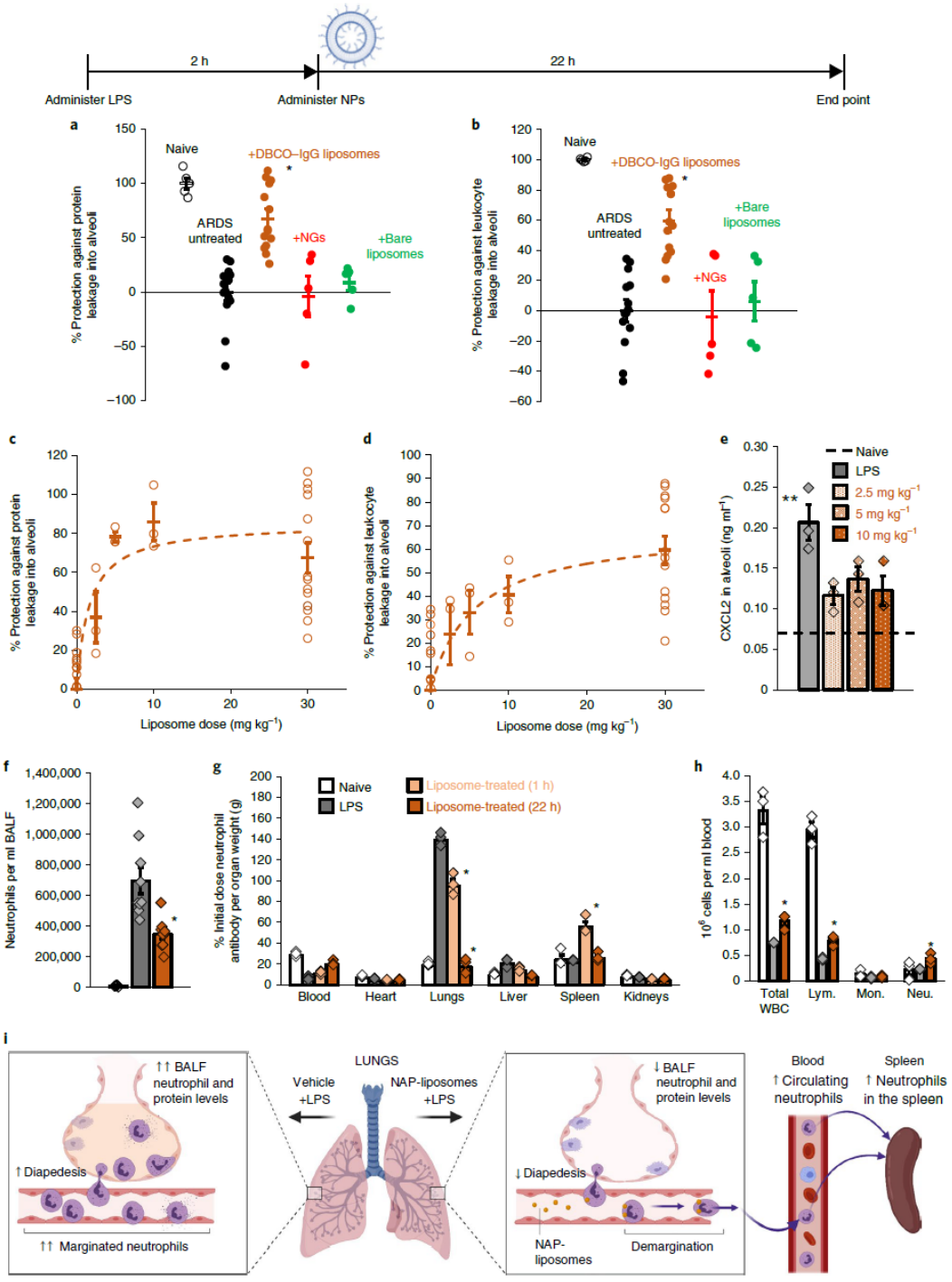

To be continued

Key Data

Effects of NAPs in model ARDS

Timeline: nanoparticles or vehicle were administered as an i.v. bolus 2 h after nebulized LPS administration (liposome schematic created with BioRender.com). **a**,**b**, BALF was harvested 22 h after nanoparticle (30 mg kg−1) or vehicle administration. **a**, Protein concentration in BALF, reflecting quantity of oedema in naive mice (n = 5 animals), sham-treated mice with model ARDS (n = 15 animals) and mice with model ARDS treated with DBCO–IgG liposomes (n = 14 animals), NGs (n = 5 animals) or bare PEGylated liposomes (n = 5 animals). *P = 6.6 × 10−7, 0.0001 and 0.002 for comparison of DBCO–IgG liposome treatment with sham treatment, NG treatment and bare liposome treatment, respectively. **b**, Concentration of leukocytes in BALF for same groups as in **a**. *P = 1.1 × 10−6, 0.0001 and 0.002 for comparison of DBCO–IgG liposome treatment with sham treatment, NG treatment and bare liposome treatment, respectively. Quantities in **a** and **b** are represented as degree of protection against infiltration into alveoli, extrapolated from levels in naive mice (100% protection) and untreated mice with model ARDS (0% protection). **c**,**d**, Dose–response for oedema (**c**) and leukocyte infiltration (**d**) in alveoli of ARDS mice treated with DBCO–IgG liposomes. Data were obtained as in **a** and **b**, but with different liposome doses (n = 3 animals for 2.5, 5 and 10 mg kg−1 liposome doses). **e**, Chemokine CXCL2 levels in alveoli of LPS-injured mice with and without DBCO–IgG liposome treatment (n = 3 animals for all groups). Dashed line indicates CXCL2 levels in alveoli of naive mice. **P = 0.024, 0.079 and 0.034 for comparison of sham treatment with 2.5, 5 and 10 mg kg−1 DBCO–IgG liposome treatment, respectively. **f**, Concentration of neutrophils in BALF of naïve mice (n = 5 animals), mice with model ARDS (n = 9 animals) and mice with model ARDS dosed with 30 mg kg−1 DBCO–IgG liposomes (n = 9 animals). For comparison of DBCO–IgG liposome treatment to sham treatment, *P = 0.009. **g**, Biodistributions of anti-Ly6G antibody in naive mice (n = 3 animals), LPS-injured mice (n = 3 animals) and mice treated with 10 mg kg−1 DBCO–IgG liposomes, with organs sampled at 1 h after treatment (n = 3 animals) or 22 h after treatment (n = 3 animals). Naive and untreated LPS-affected data are identical to data in Supplementary Fig. 1a. *P < 1 × 10−10 for all comparisons of anti-Ly6G uptake in lungs or spleen of liposome-treated mice versus sham-treated mice. **h**, Complete blood count analysis of circulating leukocyte concentrations in naive mice (n = 3 animals), LPS-injured mice (n = 3 animals) and mice treated with 10 mg kg−1 DBCO–IgG liposomes, with blood sampled 22 h after treatment (n = 3 animals). *P = 0.019, 0.025 and 0.047 for comparison of DBCO–IgG liposome-treated to sham-treated values for total white blood cell (WBC), lymphocyte (Lym.) and neutrophil (Neu.) counts, respectively. **i**, Schematic for the fate of neutrophils in mice with model ARDS, with and without DBCO–IgG liposome treatment, based on data in **f**–**h** (created with BioRender.com). Statistical significance in **a**, **b**, **e** and **f** is derived from one-way ANOVA with Tukey's multiple-comparisons test. Statistical significance in **g** and **h** is derived from two-way ANOVA with Tukey's multiple-comparisons test. All error bars indicate mean ± s.e.m.